Bragg reflection waveguide twin-beam lasers

2013 Laser Phys. 23 105802

(http://iopscience.iop.org/1555-6611/23/10/105802)

Laser Phys. **23** (2013) 105802 (5pp) doi:10.1088/1054-660X/23/10/105802

Bragg reflection waveguide twin-beam lasers

Lijie Wang[1,2], Cunzhu Tong[1], Yugang Zeng[1], Ye Yang[1], Hangyu Peng[1], Sicong Tian[1], Hao Wu[1] and Lijun Wang[1]

[1] State Key Laboratory of Luminescence and Application, Changchun Institute of Optics, Fine Mechanics and Physics, Chinese Academy of Sciences, Changchun 130033, People's Republic of China
[2] University of Chinese Academy of Sciences, Beijing 100049, People's Republic of China

E-mail: tongcz@ciomp.ac.cn

Received 24 April 2013
Accepted for publication 29 July 2013
Published 16 August 2013
Online at stacks.iop.org/LP/23/105802

Abstract
We report on an edge-emitting diode laser with an ultra-narrow twin-lobed far field based on a dual-sided Bragg reflection waveguide. Lasers with a stripe width of 10 μm exhibit two stable near-circular beams symmetrically located at about $\pm 31^\circ$ with full width at half maximum (FWHM) of 7.2° and 5.4° respectively in the vertical and lateral directions. The mechanism behind the achievement of the twin-beam output is presented, and the symmetry of these two beams is analyzed by comparing the beam FWHM and power distribution. Single longitudinal mode operation is achieved and periodic spectral modulation is observed.

(Some figures may appear in colour only in the online journal)

1. Introduction

Lasers with stable and symmetrical dual-beam output are in demand for a wide variety of applications, including high speed laser scanning [1, 2], high sensitivity laser absorption spectroscopy [3, 4], advanced laser (speckle or particle) velocimetry [5, 6] and trench depth monitoring [7]. There are two general approaches for generating dual laser beams: one approach is to couple the beams from two individual lasers using an optical fiber array or beam-combiner; the other approach is to split one incident beam into two beams by using a diffraction grating, a polarization prism, a nondegenerate optical parametric oscillator [8] or external feedback [9]. Application of the former approach is limited by the complicated optical alignment and non-compact size. The twin-stripe diode lasers or the phase-locked diode laser array operating in the out-of-phase mode can produce a double-lobed far field (FF) in the lateral direction [10]; however, these lasers suffer from serious instabilities resulting from the thermal effects generated by adjacent elements during operation.

The ideal method to achieve dual-beam laser output is based on the waveguide structure of the laser device, which enables a compact size and cheap fabrication. The use of the photonic bandgap (PBG) effect of a photonic crystal is a promising way to control the electric field distribution on the laser output facet, which determines the FF beam pattern. Two-dimensional photonic crystal surface-emitting lasers have previously been reported that are capable of producing a range of beam patterns [11]. In recent years, edge-emitting diode lasers based on double-sided quarter-wave Bragg reflection waveguides (QtW-BRWs) or so-called one-dimensional photonic crystals have been developed, whose vertical FF distribution shows two main lobes with many side peaks [12–14]. However, for QtW-BRWs in which the layers of the Bragg reflectors have a thickness equal to one-quarter of the transverse vector component of the guided mode, the PBG mode is placed in the center of the stop band, which results in maximum confinement of the optical field in the core defect layer. This tight confinement of the optical mode will lead to large beam divergence and a strong power distribution in the central side-lobes, restricting the optical coupling efficiency [12, 13]. In order to achieve narrow vertical FF divergence, a large vertical spot size is required by reducing the optical confinement factor of the guided mode. More recently, the idea of using

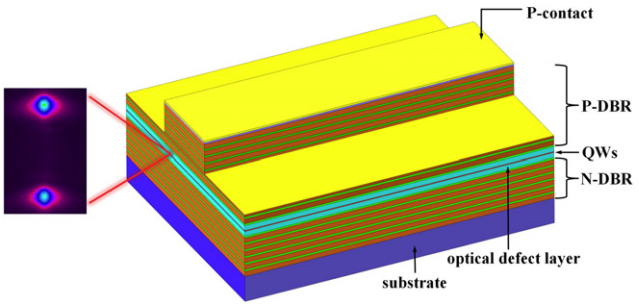

Figure 1. Schematic diagram of the BRL with a narrow twin-lobed FF.

a single-sided non-quarter-wave (non-QtW) BRW structure with no p-side periodic waveguide has been promoted to realize high power diode lasers with a narrow dual-lobed FF in the vertical direction [15]. However, as it is limited by total internal reflection in the p-side, the main problem of this approach is the bad symmetry of the two lobes and the large intensity distribution in the central part between them. In this paper we demonstrate an ultra-narrow twin-beam output using specially designed double-sided non-QtW-BRWs. The detailed mechanism for achieving the twin-beam lasing is presented. Moreover, the current-dependent spot shape and power symmetry of these two beams are studied in detail. The device exhibits a narrow spectral linewidth and a spectral modulation effect with a mode spacing of 3.3 nm.

2. Device design and fabrication

Figure 1 shows the schematic structure of the BRW laser (BRL), which consists of an optical defect layer sandwiched between the top and bottom distributed Bragg reflectors (DBR). The active region is placed in the center of the defect layer. The cladding DBR is made up of periodically alternating high and low index materials with index n_1 and n_2, respectively. When the propagation constant lies within the stop band of the BRW, the guided mode can exist even if the effective index n_{eff} is lower than the lowest index of the DBR. So the PBG guidance mechanisms can be divided into two regimes, which are respectively $n_1 > n_{\text{eff}} > n_2$ and $n_{\text{eff}} < n_2$ [16]. In order to achieve a dual-lobed FF, the Bragg form of PBG guidance ($n_{\text{eff}} < n_2$) should be utilized, in which case light propagates in all layers. Furthermore, in this work the double-sided non-QtW BRL structure is utilized in order to extend the vertical optical field significantly. This large mode expansion will reduce the FF divergence and at the same time reduce the optical density on the facet, which consequently increases the threshold for catastrophic optical mirror damage (COMD).

The refractive index profile of the designed BRL is shown in figure 2(a). Each of the top and bottom DBRs consists of six pairs of $Al_{0.1}Ga_{0.9}As/Al_{0.3}Ga_{0.7}As$ layers. The thickness of one pair of layers is 100 nm/750 nm respectively. The defect layer is 1.5 μm thick $Al_{0.3}Ga_{0.7}As$, which ensures that the effective index n_{eff} is lower than the lowest refractive index of the BRW. The gain material is two $In_{0.2}Ga_{0.8}As/GaAs$ quantum wells (QWs) designed for emission near 980 nm.

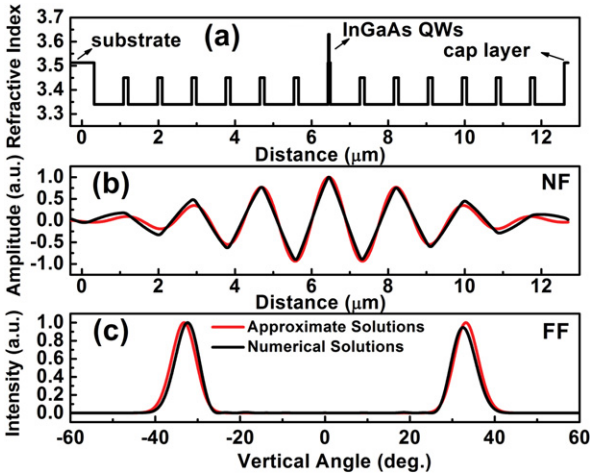

Figure 2. (a) Refractive index profile of the BRL heterostructure. (b) Calculated vertical near field (NF) electric field distribution. (c) Calculated FF curves of the fundamental mode by exact numerical solutions (black line) and approximate analytical simulations (red line).

All interfaces are linearly graded in composition over 20 nm to reduce the electrical resistance of the device. The total epitaxial thickness of the BRL is 12.7 μm.

As it uses the PBG guiding mechanism, the BRL can be designed to possess very strong mode discrimination, in which case only the fundamental mode is localized at the defect layer while all high-order modes are extended over the entire BRW and penetrate into the substrate and the contact layer. This results in large losses and low modal gain of high-order modes, allowing for stable single transverse mode operation. Figure 2(b) shows the calculated vertical near field (NF) electric field distribution of the designed BRL using exact numerical solutions. The calculated effective index of the fundamental mode is 3.327, which is lower than the low index layer of the DBR. As can be seen, the NF profile yields discrete peaks separated by nulls corresponding to an optical intensity equal to zero, and the peak intensities go down nearly exponentially from the active area to each side. The numerically calculated FF distribution in the vertical direction is given in figure 2(c), which shows two pronounced lobes symmetrically located at about $\pm 32°$. The full widths at half maximum (FWHMs) of the two lobes are respectively 6.36° and 6.54° in theory, and the intensity of the upper lobe towards the substrate is a little higher than that of the bottom lobe towards the top Bragg reflectors; this is due to the structure not being perfectly symmetrical: one side is the thick high-index substrate whereas the other side is air. Increasing the number of pairs of layers in the DBR or a inserting low index cladding layer could effectively improve the symmetry of the two lobes.

To clarify the mechanism behind the twin-beam output, the following analysis is presented. As is known, the FF radiation pattern is determined by the Fourier transformation of the NF electric field distribution. For a NF with periodic local maxima and nulls, it can be approximated by a sinusoidal or cosine function [17]. In the case of our BRL, the vertical

electric field distribution at the facet can be approximated to a cosine function multiplied by a Gaussian function:

$$E_{\mathrm{NF}}(x) = E_{\mathrm{NF}}(0)\cos\left[2\pi\frac{x}{2\Lambda}\right]\mathrm{Gaus}\left(\frac{x}{w}\right), \qquad (1)$$

where $\mathrm{Gaus}(x) = \exp(-\pi x^2)$ describes the Gaussian function, x is the transverse distance from the central active region, w is the vertical spot radius determined by the waveguide thickness, $E_{\mathrm{NF}}(0)$ is the electric field amplitude at the center of the BRL and Λ is the period width of the Bragg reflectors.

Using the Rayleigh–Sommerfeld diffraction integral $I_{\mathrm{FF}}(\theta) \propto \left|\cos\theta \int_{-\infty}^{\infty} E_{\mathrm{NF}}(x)\exp(-\mathrm{i}k_0 x\sin\theta)\mathrm{d}x\right|^2$, we can get the corresponding FF intensity distribution:

$$I_{\mathrm{FF}}(\theta) \propto \left|\frac{E_{\mathrm{NF}}(0)w\cos\theta}{2}\right|^2 \times \left|\mathrm{Gaus}\left[w\left(\frac{\sin\theta}{\lambda}-\frac{1}{2\Lambda}\right)\right] + \mathrm{Gaus}\left[w\left(\frac{\sin\theta}{\lambda}+\frac{1}{2\Lambda}\right)\right]\right|^2, \qquad (2)$$

where θ is the FF angle, $k_0 = 2\pi/\lambda$ is the free-space wavenumber and λ is the free-space wavelength.

Following equation (2), the FF intensity distribution of the BRL can be obtained; this consists of two Gaussian-shaped lobes centered respectively at $\theta = \pm\arcsin[\lambda/(2\Lambda)]$. This means that the period thickness of the DBR determines the angle of separation of the two beams. The FF divergence angle of individual lobes is primarily dependent on the vertical spot size w, which becomes narrower with the increase in w. Therefore, the angular position and divergence angle of the twin beams can be precisely controlled by engineering the BRL structure due to the advanced epitaxial growth technology. In our designed device, the period of the DBR containing the graded index layer is $\Lambda = 0.89$ μm, and $2w$ is approximately equivalent to the total waveguide thickness of the BRW. The simulated NF and FF distributions of the BRL by the approximate expressions are shown in figures 2(b) and (c), respectively (by red lines), being in excellent agreement with the numerical simulation results. Therefore, this empirical formula can provide an approximate description of the behavior of this BRL.

The BRL wafer was grown on an n+GaAs(100)-oriented substrate by an Aixtron-200 metal–organic chemical vapor deposition (MOCVD) system. After the growth, ridge waveguides of 10 μm width were defined using conventional photolithography and wet etching. The etching depth was about 3 μm. Then 200-nm SiO_2 electrical insulating layer was deposited and contact window opening was done, followed by standard p-side metallization, substrate thinning and n-side metallization. Finally, individual ridge lasers with a cavity length of 1.4 mm were cleaved and measured without any facet coating or soldering.

3. Experimental results and discussion

Figure 3 shows the light–current–voltage (*L–I–V*) characteristics of the uncoated ridge BRLs under continuous-wave (CW) and quasi-CW (QCW, pulse width = 200 μs, repetition rate = 1 kHz) operation at room temperature (RT). As can be seen, the threshold current I_{th} is about 135 mA, and the QCW output power exceeds 300 mW from two facets. The CW output power of 85 mW from two facets is achieved at 410 mA current, limited by the thermal roll-over. Higher output powers could be expected for packaged devices due to better heat conduction.

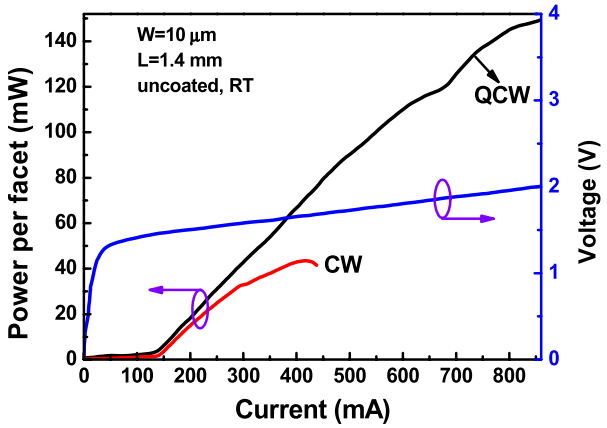

Figure 3. *L–I–V* characteristics of the uncoated ridge BRL under QCW operation (pulse width = 200 μs, repetition rate = 1 kHz) and CW operation.

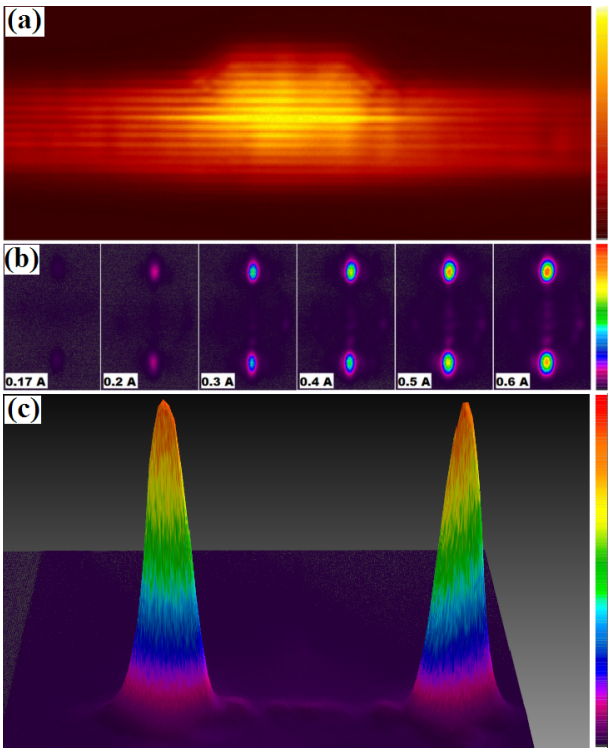

Figure 4. (a) Measured NF patterns of the ridge BRL above threshold current. (b) Measured FF patterns of the ridge BRL at various currents. (c) Measured three-dimensional FF patterns at 0.7 A current.

The NF and FF intensity patterns of the BRL were measured with camera-based profilers under QCW operation. Figure 4(a) shows the measured NF pattern, which is

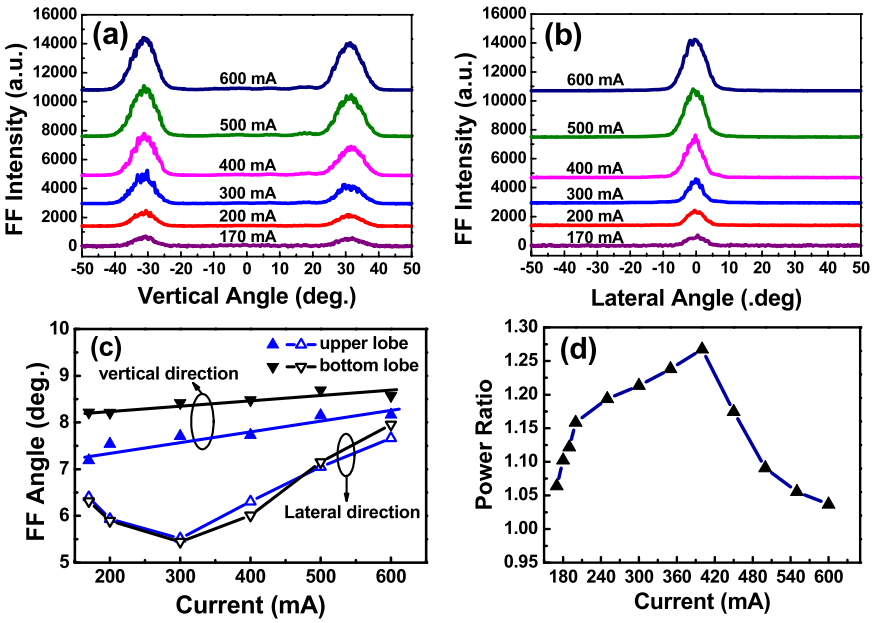

Figure 5. Measured (a) vertical FF and (b) lateral FF distribution of the ridge BRL. (c) Measured FF divergence angle (FWHM) of the upper and bottom lobes in the vertical (filled triangle) and lateral (empty triangle) direction as a function of injected current. (d) The power ratio of the upper lobe versus the bottom lobe at different currents.

composed of a big bright peak in the center surrounded by periodically discrete peaks separated by dark lines. This is consistent with the theoretical result shown in figure 2(b). In addition, the transverse optical field extends significantly into the thick multilayer waveguide, which is crucial for narrowing the FF divergence and reducing the catastrophic optical damage. The measured FF emission patterns of the BRL at different currents were shown in figure 4(b). As one can see, the FF along the vertical direction exhibits two distinct lobes with a large separation, which contains nearly the total radiated power. The vertical beam width remains very stable and no obvious intensity redistribution takes place with the increase in current. These measured results indicate the stable single transverse mode operation of the BRL. Figure 4(c) illustrates the three-dimensional radiation pattern of the BRL under 0.7 A current, which shows a narrow twin-beam output. The field intensity in the central part between the two beams is negligibly low, and these two beams show almost the same shape and power. Therefore, the present work shows a very significant improvement over the previous Qtw-BRW lasers.

Figure 5(a) shows the measured vertical FF distribution of the BRL at various currents. The FF consists of two narrow lobes symmetrically located at about $\pm 31°$, and the FWHM of individual lobes and the separation angle between the two lobes were almost independent of the current. Furthermore, the field intensity of the upper lobe at about $-31°$ is a little stronger than that of the bottom lobe at about 31°, being consistent with the numerical simulation result shown in figure 2(c). The large separation angle of these two beams allows the respective control of both beams with the optical elements, such as the collimator lens, optical modulator, half wave plate or optical feedback mirror, which will enhance the flexibility of realistic applications. For instance, twin beams with a large separation angle can simplify the off-axis external cavity laser, in which case strong feedback is provided on one beam by using reflective diffraction gratings while the other beam is coupled out completely [9]. Thus, more power will be concentrated in the out-coupled beam, and wavelength stabilization and tunability could be achieved. Furthermore, this narrow twin-beam emission can be easily converted to two parallel beams by a fast-axis collimator lens; these could be used as the compact sources for dual-beam scanning or dual-beam laser interferometry for applications in high speed scanning or *in situ* depth monitoring.

As shown in figure 5(b), the lateral far field profile remains a clear Gaussian distribution without filamentation up to 600 mA. This proves that the BRL enables fundamental lateral mode operation even for 10 μm wide ridge stripes, due to the ultra-thick vertical waveguide of the BRL. This large vertical mode expansion will lead to weaker interaction of the optical field with the ridge edges and the active area, which could suppress higher order lateral mode lasing and reduce the generation of beam filamentation [18, 19].

Figure 5(c) shows the beam divergence angles in the vertical and lateral directions at different injected currents. The vertical divergence angles of the upper and bottom lobes are, respectively, 7.2° and 8.2° (FWHM) at 170 mA current and increase by no more than 1° up to 600 mA. In the lateral direction, the FWHM beam divergence angles of both lobes are nearly the same. It first reduces from 6.4° at 170 mA to 5.4° at 300 mA, which might be because the lateral current spreading gives rise to a realistic gain width with increasing current. Then the lateral FF angle (FWHM) increases slightly to about 8° at 600 mA current. The increase in the lateral beam divergence is caused by the thermally induced increase in the refractive index of the ridge waveguide. The ratio between the vertical and lateral FF angles is lower than 1.6 over the full operating range and is close to 1 for a high injection current.

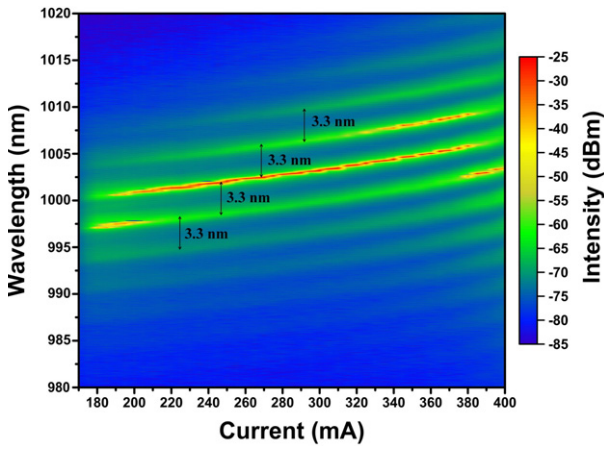

Figure 6. Color-scale mapping of the optical spectrum versus injected current for the ridge BRL.

This near circular shaped beam profile can greatly increase the optical coupling efficiency.

To quantify the power symmetry of these two lobes, the power ratios of the upper lobe versus the bottom lobe at different currents were measured and are shown in figure 5(d). It increases first from 1.06 at 170 mA to 1.16 at 200 mA. Then the increasing rate reduces, and the ratio reaches its maximum value (∼1.27) at 400 mA. After that, the ratio decreases and tends to 1, indicating that the power of two lobes tends to be equal. This double well-correlated laser beam can be used as signal and reference beam, respectively, to effectively reduce the intensity noise in laser absorption measurements.

The lasing spectra of the ridge BRLs were measured in CW mode by an ANDO AQ6317B optical spectrum analyzer. Figure 6 shows the experimental logarithmic scaled spectral map at numerous currents with a step width of 5 mA. The ridge BRL achieves a very narrow spectral linewidth of about 0.05 nm (FWHM) limited by the measurement resolution. This single longitudinal mode emission could also verify that the laser operates in single transverse mode. In addition, the BRL exhibits a quite pronounced spectral modulation superimposed on the normal longitudinal Fabry–Perot modes. The wavelength separation is approximately 3.3 nm, which is much larger than the longitudinal mode spacing (∼0.09 nm). It can also be seen that the peak wavelength is 1000.86 nm at 200 mA, and then as the current increases the other mode with a wavelength of 1006.82 nm starts to reach threshold condition and dominate the lasing at around 320 mA. The appearance of such a mode hop is due to thermal detuning of the gain and reflector sections [20], which is usually connected with a kink in the *L–I* characteristics of the laser.

4. Conclusion

In summary, we have demonstrated a narrow twin-beam laser output from a dual-sided BRW diode laser. Nearly the entire emitted power of the BRL is concentrated in the two lobes located at about ±31° in the vertical direction, while the FWHM in the vertical FF of both lobes is as narrow as 7.2°. We believe that this laser with controllable, symmetrical and nearly circular shaped twin-beam emission will be of great interest for dual-beam laser applications.

Acknowledgments

This work was supported by the financial support from the National Natural Science Foundation of China under grant nos 61076064 and 61176046, the Hundred Talents Program of Chinese Academy of Sciences, and the Open Project of the State Key Lab on Integrated Optoelectronics (no. 2011KFB006).

References

[1] Arimoto A, Saitoh S, Mochizuki T, Kikuchi Y and Hatazawa K 1987 *Appl. Opt.* **26** 2554
[2] Kataoka K 2008 *Opt. Rev.* **15** 196
[3] Heidmann A, Horowicz R J, Reynaud S, Giacobino E, Fabre C and Camy G 1987 *Phys. Rev. Lett.* **59** 2555
[4] Thanh N T K, Rees J H and Rosenzweig Z 2002 *Anal. Bioanal. Chem.* **374** 1174
[5] Kawahashi M and Hosoi K 1991 *Exp. Fluids* **11** 278
[6] Wang B B, Liao Q, Bootsma H A and Wang P F 2012 *Exp. Fluids* **52** 1401
[7] Amary P and Cattelan D 2003 A new polarimetric camera for real-time trench depth monitoring in micromachining applications *Readout* **7** 82
[8] Hayasaka K, Zhang Y and Kasai K 2004 *Opt. Lett.* **29** 1665
[9] Jechow A, Lichtner M, Menzel R, Radziunas M, Skoczowsky D and Vladimirov A G 2009 *Opt. Express* **17** 19599
[10] Chun M K, Whitman T L and Soenksen D G 1987 *Appl. Opt.* **26** 4518
[11] Miyai E, Sakai K, Okano T, Kunishi W, Ohnishi D and Noda S 2006 *Nature* **441** 946
[12] Bijlani B J and Helmy A S 2009 *Opt. Lett.* **34** 3734
[13] Tong C Z, Bijlani B J, Zhao L J, Alali S, Han Q and Helmy A S 2011 *IEEE Photon. Technol. Lett.* **23** 1025
[14] Zareian N, Abolghasem P and Helmy A S 2011 *J. Lightwave Technol.* **29** 728
[15] Wang L J, Yang Y, Zeng Y G, Wang L J, Tong C Z, Shan X N, Zhao H X, Wang R and Yoon S F 2012 *Appl. Phys.* B **107** 809
[16] Cregan R F, Mangan B J, Knight J C, Birks T A, Russell P St J, Roberts P J and Allan D C 1999 *Science* **285** 1537
[17] Bai Y, Slivken S, Darvish S R, Haddadi A, Gokden B and Razeghi M 2009 *Appl. Phys. Lett.* **95** 221104
[18] Maximov M V *et al* 2008 *IEEE J. Sel. Top. Quantum Electron.* **14** 1113
[19] Pietrzak A, Wenzel H, Crump P, Bugge F, Fricke J, Spreemann M, Erbert G and Trankle G 2012 *IEEE J. Quantum Electron.* **48** 568
[20] Feise D, John W, Bugge F, Blume G, Hassoun T, Fricke J, Paschke K and Erbert G 2012 *Opt. Lett.* **37** 1532